Epitope and functional classification of human neutralizing antibodies against SFTSV Gn

Qianran Wang[1#], Hao Li[2#], Fanchong Jian[3], Aoxiang Han[2], Yuanni Liu[4], Jingyi Liu[1,5], Yuanling Yu[1], Jing Wang[1], Lingling Yu[1], Yanxia Wang[1], Haiyan Sun[1], Miaomiao Ma[1], Fei Shao[1], Liuluan Zhu[6]*, Wei Liu[2]*, Yunlong Cao[1,3,7,8]*

[1]Changping Laboratory, Beijing, P.R. China.

[2]State Key Laboratory of Pathogen and Biosecurity, Academy of Military Medical Sciences, Beijing, P.R. China.

[3]Biomedical Pioneering Innovation Center (BIOPIC), School of Life Sciences, Peking University, Beijing, China.

[4]Department of Infectious Diseases, Yantai Qishan Hospital, Yantai, P.R. China.

[5]College of Future Technology, Peking University, Beijing, P. R. China.

[6]Beijing Key Laboratory of Viral Infectious Diseases, Beijing Ditan Hospital, Capital Medical University, Beijing, P.R. China.

[7]Peking-Tsinghua Center for Life Sciences, Peking University, Beijing, P.R. China.

[8]Lead contact

[#]These authors contributed equally.

*Correspondence: yunlongcao@pku.edu.cn (Y.C.), liuwei@bmi.ac.cn (W.L.), zhuliuluan@ccmu.edu.cn (L.Z.)

SUMMARY

Severe fever with thrombocytopenia syndrome virus (SFTSV) is a lethal bunyavirus lacking approved countermeasures. From SFTS survivors, we isolated 84 human monoclonal antibodies (mAbs) against the viral glycoproteins Gn and Gc. Gn-specific mAbs demonstrate superior neutralization breadth and potency compared to the restricted neutralizing activity observed with Gc. Using a high-throughput yeast display deep mutational scanning (DMS) platform, we classified Gn-head mAbs into eight epitope groups, among which four groups (IA, ID, IIIA, IIIB) conferring neutralization. Notably, mAbs BD70-4003 (group IA) and BD70-4017 (group IIIA) exhibited broad neutralization and provided 100% protection in a lethal mouse model. Cryo-EM structural analysis of these mAbs in complex with the Gn-head revealed their binding interfaces, directly validating the epitope residues identified by DMS. Our study delineates the antigenic landscape of SFTSV Gn, identifies potent therapeutic candidates, and establishes DMS coupled with structural validation as a powerful framework for antibody discovery against bunyavirus.

INTRODUCTION

Severe fever with thrombocytopenia syndrome virus (SFTSV), or *Bandavirus dabieense*, is an emerging tick-borne phlebovirus first identified in China in 2009 and has since reported across East and Southeast Asia, including Japan, South Korea, Vietnam, Pakistan, and Thailand.[1-3] Clinical manifestations range from fever, thrombocytopenia, and leukopenia to multi-organ dysfunction, with a subset of patients developing hemorrhagic symptoms and organ failure. The case fatality rate (CFR) is approximately 16.2% (95% CI 14.6-17.8) among confirmed cases.[4-6] The principal vector, the Asian longhorned tick, has recently been detected in North America, Russia, and Australia, raising concerns regarding geographic expansion and the increasing risk of human-to-human transmission.[7-9] Despite its designation by the World Health Organization as a priority pathogen requiring urgent countermeasures, no licensed vaccines or effective antiviral drugs are currently available.

The tripartite SFTSV genome encodes a glycoprotein precursor on the M segment, which is cleaved into Gn and Gc subunits that mediate receptor binding and membrane fusion during viral entry.[10,11] These glycoproteins are the primary mediators of viral entry; Gn is generally implicated in initial

receptor attachment, while Gc facilitates the low-pH-dependent fusion of the viral and endosomal membranes. These Gn/Gc heterodimers organize into higher-order hexon and penton structures, creating a dense and ordered lattice that covers the viral envelope.[12]

Recent structural biology breakthroughs have suggested that the Gn glycoprotein as an immunodominant target for neutralizing antibodies (mAbs).[12] The Gn ectodomain consists of a globular head and a stem region. The Gn-head (residues 20-340) is further subdivided into three distinct structural domains: Domain I, Domain II, and Domain III. Domain I is characterized by high surface exposure and is believed to harbor the critical interfaces for host receptor engagement. Domain II acts as a β-connector structure, while Domain III forms a structural "cap" that partially shields the fusion loop of the Gc subunit, thereby regulating the timing of membrane fusion. The preservation of these domains across diverse SFTSV clades makes them attractive targets for the development of universal therapeutics and vaccine antigens.

Multiple monoclonal antibodies (mAbs) against Gn have been described, but their epitopes, potency, and breadth vary significantly.[13-19] A systematic evaluation is essential to delineate the precise relationship between Gn-directed antibody epitopes and neutralization potency, both *in vitro* and *in vivo*, to inform the development of therapeutics and vaccines. Deep mutational scanning (DMS) technology enables epitope mapping with significantly higher efficiency and resolution than traditional binning techniques.[20,21] We previously developed a high-throughput epitope mapping platform based on DMS to study SARS-CoV-2, establishing a pipeline to isolate large panels of mAbs and simultaneously identify their precise binding epitopes.[22-27] Here, we applied this technology to SFTSV to elucidate the intrinsic relationship between antigenic epitopes and functional antibody profiles.

We report the isolation and epitope classification of human mAbs from SFTSV convalescents. We assessed binding and neutralization using enzyme-linked immunosorbent assay (ELISA), pseudovirus assays, and authentic virus neutralization assays. Using a novel yeast DMS approach adapted for bunyaviruses, we classified Gn-head mAbs into eight epitope groups (IA-ID, IIA-IIB, IIIA-IIIB). Four groups (IA, ID, IIIA and IIIB) demonstrated neutralizing activity. Two antibodies in particular—BD70-4003 (IA) and BD70-4017 (IIIA)—exhibited broad neutralization and

77 provided 100% protection in mice, making them promising drug candidates. Cryo-electron
78 microscopy (cryo-EM) structural analyses of three mAbs (BD70-4003, BD70-4008 and BD70-4017)
79 defined the molecular basis of recognition and verified the accuracy of our DMS system. Our results
80 elucidate the overall epitope distribution of the SFTSV Gn-head domain and identify highly potent
81 neutralizing antibodies targeting distinct epitopes, providing theoretical guidance for future
82 therapeutic and vaccine design.

83 **RESULTS**

84 **Isolation of mAbs from SFTS convalescents**

85 We collected whole-blood samples from 12 SFTSV survivors who had been infected for more than
86 one year (Table S1). Serum samples were analyzed for viral Gn/Gc-specific IgG titers and for
87 neutralizing activities against SFTSV pseudovirus. The results showed that Gn or Gc reactive
88 antibody remained at high levels in these serum samples (Figure 1A), and the serum exhibited high
89 neutralizing activity against six pseudovirus strains (Figure 1B). This is consistent with previous
90 reports that SFTSV glycoproteins induce long-lasting antibodies, and also suggests the possibility
91 of potentially broadly neutralizing antibodies.[28,29]

92 To isolate monoclonal antibodies, we purified antigen-specific memory B cells from peripheral
93 blood mononuclear cells (PBMCs) using fluorescence-activated cell sorting (FACS). From the
94 PBMCs, $CD19^{+}$ IgM^{-} $CD27^{+}$ memory B cells were stained simultaneously with HB29 Gn and Gc
95 glycoproteins, and cells positive for either antigen were sorted as antigen-specific B cells (Figure
96 S1A). To distinguish Gn- and Gc- specific responses during sequencing, each antigen was labeled
97 with a unique DNA barcode. In total, we retrieved 1,316 paired heavy-light chain antigen-specific
98 antibody sequences via high-throughput single-cell V(D)J sequencing.

99 A subset of antibody sequences was randomly selected for expression and further functional
100 characterization. In total, we expressed 54 Gn-specific and 44 Gc-specific IgG1 antibodies *in vitro*.
101 ELISA confirmed binding activity in 49/54 (90.7%) of the Gn group and 35/44 (79.5%) of the Gc
102 group (Table S2). ELISA-positive Gn (n = 49) and Gc (n = 35) mAbs were subsequently subjected
103 to neutralization assays.

104 In the neutralization assay, we employed 9 vesicular stomatitis virus (VSV)-based pseudovirus
105 strains representing six major SFTSV genotypes (A–F) (Table S3-S6).[30-32] These strains include:
106 HB29 (genotype D), HBMC16 (genotype D), WCH (genotype A), HN13 (genotype A), HN20
107 (genotype F), G/K/2012 (genotype F), SD4 (genotype E), SPL030A (genotype B), and AHL
108 (genotype C). The results show that mAbs against Gn exhibited more potent neutralization effects
109 against the pseudovirus than those against Gc, which is consistent with previous reports that
110 neutralizing antibodies against SFTSV primarily target the Gn antigen (Figures 1C and 1D).[14,33-35]
111 This observation was further validated in authentic virus neutralization assays, where eleven
112 selected Gn-specific pseudovirus neutralizing mAbs—but zero Gc-specific mAbs—showed greater
113 than 50% inhibition against the HBMC strain at 0.25 μg/mL (Figure S1B). Based on these results,
114 we confirm that Gn is the immunodominant antigen target for SFTSV neutralizing antibodies.

115 **Epitope mapping via deep mutational scanning**

116 Defining antibody epitopes is essential for understanding neutralization mechanisms and for
117 identifying functionally important regions on viral antigens that can be targeted for therapeutic or
118 vaccine development. To provide a high-resolution epitope map of the Gn antigenic surface, a
119 comprehensive deep mutational scanning (DMS) platform was implemented.[21,36-38] A yeast display
120 library of the HB29 Gn-head domain (residues 20-340) was constructed, incorporating nearly all
121 possible amino acid substitutions at each position. By subjecting this library to antibody selection
122 and high-throughput sequencing of escape variants, critical binding residues were identified for 44
123 newly isolated human Gn-mAbs and several benchmark control antibodies. Specially, we performed
124 negative selection FACS to isolate yeast cells that failed to bind specific antibodies, followed by
125 sequencing to identify critical escape mutants. Unsupervised clustering of the resulting escape
126 profiles partitioned the Gn-head into eight distinct epitope groups, providing a systematic
127 framework for understanding antibody function.

128 The eight epitope groups (IA-ID, IIA-IIB, IIIA-IIIB) demonstrate a diverse distribution across the
129 Gn-head structure (Figures 2A-C, Figure S2). Groups IA, IC, and ID are localized to Domain I.
130 Group IA, represented by elite neutralizing mAbs such as BD70-4003, targets a surface-exposed
131 region involving residues D159, G161, S163-S164, and L166. Group IC (e.g., control antibody

132 SF5[39]) and ID (e.g., control antibody 40C10[16]) target distinct sites on the opposite faces of Domain
133 I. Domain II is recognized by groups IIA and IIB, which include antibodies like N1D10 and B1G11[15].
134 No convergent V(D)J gene usage was observed within mAbs targeting Domain I and II (Figures
135 2D). Despite high binding scores, antibodies targeting Domain II often exhibit poor neutralizing
136 activity, likely due to the domain's less accessible orientation on the mature virion (Figures 2E and
137 2F).

138 Group III antibodies are subdivided into IIIA and IIIB and target Domain III. Group IIIA antibodies,
139 such as BD70-4017, interact with a cluster of residues including Q73-R74, G264-P265, and E271.
140 Group IIIB antibodies, including the well-characterized MAb4-5[13], focus on an epitope involving
141 residues E271, G282, C287, K288, and C292. Notably, gene analysis of Group IIIB mAbs showed
142 frequent genes involving IGHV5-51 (Figures 2D). Importantly, comparative analysis reveals that
143 the most potent neutralizing activity is concentrated in Group IA and IIIA, followed by IIIB and ID,
144 whereas IC, IIA, and IIB are largely non-neutralizing. This trend was also consistent across another
145 eight SFTSV pseudoviruses strains, with the most potent neutralization again observed in the IA
146 and IIIA antibody groups, highlighting the functional dominance of the IA and IIIA epitopes (Figure
147 S3).

148 To validate the accuracy of our DMS platform, we compared our results with previously published
149 crystal or cryo-EM structures. It has been reported that the interface between the Gn head and
150 MAb4-5 (IIIB) was located on sites S251-F256, K275-G278, and 284-294 by crystal structure
151 analysis,[13] which was consistent with the key amino acids (C287-K288, C292) we have screened
152 (Figures 2B and 2C). For domain I antibodies SF5 (IC) and 40C10 (ID), DMS identified key
153 residues S81-A85, S123-G126, R171 for SF5, and H64-S65, K111-K113, G142 for 40C10 (Figures
154 2B and 2C). Actually, SF5 (IC) bound to sites R74-S90, G121-G126, T150-R171[39], while 40C10
155 (ID) bound to sites R62-Q66, D102, K111-S115, C156.[16] Except for site G142, which was close to
156 S65, all sites in this study were consistent with their complex structures. Results of mAbs against
157 domain II were also relatively accurate. According to Ren *et al*'s study,[15] N1D10 (IIA) and B1G11
158 (IIB) mainly bound to sites E114-G121, G218-D226, V339-N340, and P185-E193, T321-V323,
159 respectively, which also include the sites of our DMS results (Figures 2B and 2C). These

160 correlations confirm that the yeast-based DMS library effectively captures the functional epitopes
161 of SFTSV glycoproteins, providing a reliable high-throughput epitope determination alternative to
162 structural mapping.

163 **Protective effect of Gn mAbs *in vitro* and *in vivo***

164 Previous pseudovirus and authentic virus neutralization screening identified six Gn antibodies
165 (BD70-4003, BD70-4008, BD70-4009, BD70-4013, BD70-4017, and BD70-4022) with broad
166 inhibitory effects (Table S3). These elite candidates were also found to have undergone extensive
167 affinity maturation, as evidenced by high somatic hypermutation (SHM) rates and binding affinities
168 (Table S7 and Figure S4). Notably, the binding affinity of BD70-4008 and BD70-4003 against Gn
169 have reached in the low picomolar range.

170 Focus reduction neutralization test (FRNT) was performed to further validate the neutralization
171 capacity of these elite mAbs (Figure 3A).[18] All 6 Gn mAbs demonstrated potent neutralization *in*
172 *vitro* with low $FRNT_{50}$ values (Figure 3B). Interestingly, although BD70-4017 showed relatively
173 modest neutralization in the pseudovirus system compared to its peers, its performance against
174 authentic SFTSV strains was dramatically enhanced, illustrating that pseudotype assays may not
175 fully recapitulate the inhibitory potential of certain epitopes.

176 To evaluate the prophylactic and therapeutic efficacy of the 6 mAb candidates against SFTSV *in*
177 *vivo*, *IFNAR1*$^{-/-}$ mice were challenged with SFTSV before or after treatment with the mAb. In
178 prophylactic and therapeutic groups, 5 mg/kg antibody was given to the mice via intraperitoneal
179 (i.p.) injection 1 day pre-infection or 1 day post infection (dpi), respectively (Figures 3C and 3F). A
180 vehicle group of mice that received a human IgG1 isotype control antibody was also included. Each
181 group consisted of five or six mice. The body weight of each mouse in each group was monitored
182 and recorded daily. Serum samples were collected from all mice on 3 dpi, with an additional
183 collection performed for the therapeutic group on 5 dpi. And the livers, spleens, and lungs were
184 collected for viral load analyses via qRT-PCR.

185 In the prophylactic treatment group, most mice died between 5-6 dpi without mAbs injection and
186 exhibited significantly higher viral RNA copies in serum samples (Figures 3D and 3E). BD70-4003

187 (IA), BD70-4008 (IIIA), and BD70-4017 (IIIA) protected 100% mice from SFTSV infection, while
188 one mouse died on day 7 or day 10 in the groups treated with BD70-4009 (IIIA), BD70-4013 (IA),
189 and BD70-4022 (IIIA) (Figure 3D). Viral copy numbers in the serum of mice treated with BD70-
190 4003, BD70-4008, or BD70-4017 were below the detection limit, indicating that these three
191 antibodies exhibited superior efficacy in promoting viral clearance (Figure 3E).

192 In the therapeutic treatment group, BD70-4003 (IA) and BD70-4017 (IIIA) protected 100% mice
193 from SFTSV challenge (Figure 3G), and extremely low viral copy numbers were detected in the
194 serum samples collected on both 3 or 5 dpi (Figures 3H and 3I). The remaining four antibodies
195 conferred weaker protective effects, with varying numbers of deaths occurring within their
196 respective treatment groups. We also analyzed tissue samples collected on 5 dpi. Viral copy numbers
197 in spleens, livers, and lungs from the BD70-4003 and BD70-4017 treatment groups were reduced
198 by 3-4 log values compared to the vehicle group (Figures 3J, 3K, and 3L). All these results suggested
199 that administration of either BD70-4003 (IA) or BD70-4017 (IIIA) exhibited significant therapeutic
200 effects. The *in vivo* experimental results further validated our preliminary *in vitro* antibody screening
201 strategy, demonstrating that antibodies targeting epitopes IA and IIIA hold the greatest potential for
202 development as therapeutic antibodies.

203 **Structural analyses of Gn-Ab complexes**

204 To gain deeper insights into the molecular mechanisms underlying the distinct neutralizing activities
205 of different antibodies, we selected 3 mAbs (BD70-4003, BD70-4008, and BD70-4017) for
206 structural analysis. Among them, BD70-4003 and BD70-4008 exhibited competitive binding to Gn
207 protein. Consequently, except Gn head/BD70-4003 Fab and Gn head/BD70-4008 Fab, we also
208 designed 2 combinations of antibodies to form complexes with the Gn-head for structural analysis,
209 thereby increasing the complex size to facilitate structural determination. The Gn head/BD70-4003
210 Fab and Gn head/BD70-4008 Fab were detected by cryo-EM (Table S8), with their structure
211 ultimately resolved at reported global resolution with 2.85 and 2.97 Å, respectively (Figures S5A
212 and S5B). Two complexes, Gn head/BD70-4003 Fab/BD70-4017 Fab and Gn head/BD70-4008
213 Fab/BD70-4017 Fab, were also resolved with both 2.69 Å resolution (Figures S5C and S5D).

214 The complex structure of the BD70-4003 Fab bound to the Gn-head revealed a large interaction

215 interface primarily located on Domain I. Key contact residues on Gn included S32, K34, Q68, Q73-
216 R74, S145-K147, S158-G161, S163-S164, and L166-S169 (Figures 4A and 4B). The interaction is
217 stabilized by 11 hydrogen bonds, with the heavy chain (specifically residues D55, E100, D101,
218 D104, and Y105) contributing the majority of the bonding potential (Figure 4C). This epitope
219 overlaps significantly with the identified binding sites for the host receptor C-C motif chemokine
220 receptor 2 (CCR2).[40] Specifically, the proximity to residue D170, which is a critical determinant of
221 SFTSV-Gn binding to CCR2, indicates that BD70-4003 neutralizes the virus by competitively
222 inhibiting receptor attachment.[41]

223 In contrast, BD70-4017 primarily targets Domain III, engaging residues K260-T263, P265, S267-
224 E270, and A273-C280 (Figures 4D and 4E). A significant feature of the BD70-4017 binding mode
225 is its interaction with the N-linked glycan at position N63 of Domain I (Figure 4F). The light chain
226 residue T70 forms a hydrogen bond with the mannose moiety of this glycan, a mechanism that may
227 enhance the stability of the complex on the authentic virion surface. Given that Domain III acts as
228 a structural cap over the Gc fusion loop, the binding of BD70-4017 likely hinders the exposure of
229 the fusion machinery, thereby preventing the acidification-induced conformational changes required
230 for viral entry.

231 The structural analysis of BD70-4008 provided a cautionary insight into the interpretation of DMS
232 data. Although DMS clustered BD70-4008 into group IIIA along with BD70-4017, the cryo-EM
233 structure revealed that BD70-4008 actually interacts with a hybrid epitope spanning Domain I and
234 Domain III (Figure 4G-I). The discrepancy arose because BD70-4008 possesses relatively few
235 escape residues (Q50, R74, T263), which made its DMS escape profile computationally similar to
236 the Domain III-focused BD70-4017. This "grouping bias" highlights that while DMS is a powerful
237 tool for rapid classification, it can underrepresent complex, multi-domain epitopes if only a subset
238 of residues provides strong escape signals. Interestingly, although the amino acid residues on the
239 interacting interface of BD70-4008 and BD70-4017 have a slight overlap, involving 3 residues
240 (G262, T263 and P265), the combination of the two antibodies has little hindering effect on the
241 formation of the Gn head/BD70-4008/BD70-4017 complex (Figure 4J-K).

242 To investigate the neutralization mechanisms of BD70-4003, BD70-4008, and BD70-4017, we

243 superimposed the structures of the BD70-4003/BD70-4017-Gn and BD70-4008/BD70-4017-Gn
244 complexes onto the native SFTSV virion structure. Previous studies have shown that Gn-Gc
245 heterodimers form hexon and penton on the surface of SFTSV virions.[12,42] Our results showed that
246 BD70-4003/BD70-4017 and BD70-4008/BD70-4017 binding sites were located on the surfaces of
247 the hexons or pentons (Figures 5A and 5B). BD70-4003 or BD70-4008 binds to the top side of the
248 authentic SFTSV virion with an orientation nearly perpendicular to the viral membrane, which may
249 be the key factor contributing to the superior affinity and neutralization effects. Although BD70-
250 4017 binds to a more lateral position, its binding is less affected and experiences minimal steric
251 hindrance. This structural complementarity supports the potential for combining these antibodies
252 into a therapeutic cocktail.

253 **DISCUSSION**

254 Currently, the clinical management of SFTS is centered on comprehensive supportive care,
255 including platelet transfusion, intravenous immunoglobulin, and blood purification.[43-45] Due to the
256 lack of specific and effective antiviral drugs, severe cases can rapidly progress to multiple organ
257 failure, particularly in older patients, with significantly increased mortality rates.[46] In this study, we
258 successfully combined pseudovirus screening with authentic virus validation to identify potent
259 mAbs that may serves as SFTSV therapeutics.[32] Compared to authentic viruses, pseudoviruses offer
260 advantages including lower strain restrictions, higher detection throughput, and operational
261 convenience, making them suitable for preliminary efficacy screening. However, we observed that
262 antibody BD70-4017, which displayed relatively modest performance in the pseudovirus system,
263 demonstrated significantly enhanced neutralizing activity against the authentic virus (Figure 1 and
264 Table S3), highlighting that the VSV-G-based pseudovirus system cannot completely mimic the
265 surface glycoprotein arrangement of authentic SFTSV. Similar limitations have been previously
266 reported in studies on both SFTSV[15] and hantavirus[47], and lentiviral-based SFTSV
267 pseudoviruses[48,49] also appear unable to fully recapitulate authentic viral features. Future research
268 should focus on optimizing existing systems or developing novel platforms that accurately mimic
269 the glycoprotein distribution of the authentic virus, thereby enabling high-throughput antibody
270 testing in conventional laboratory settings.

Mapping antibody epitopes is essential for understanding neutralization mechanisms and guiding rational vaccine and therapeutic design. The implementation of a high-resolution DMS platform for bunyavirus antibody characterization represents a significant technical advancement. Traditional epitope mapping methods, such as competitive ELISA or cross-blocking assays, provide only coarse-grained information about epitope groups. In contrast, DMS provides residue-level specificity, allowing for the immediate identification of potential escape variants and the rational design of antibody cocktails. By comprehensively evaluating the impact of every possible amino acid substitution on antibody binding, researchers can proactively monitor viral antigenic evolution in the field and update therapeutic strategies accordingly. Also, the revision of the SFTSV Gn antigenic landscape into eight specific epitope groups clarifies why previous studies observed varying degrees of protection. For instance, targeting the variable regions of Domain III (IIIB) often leads to strain-specific or weak protection compared to the functional interfaces in Domain III (IIIA).

The identification of the BD70 series coincides with a burgeoning field of SFTSV immunology characterized by the discovery of several other potent human and murine antibodies.[13-17] Recent studies have introduced several high-performing antibody series, notably the JK series (JK-2, JK-8),[18] the SD series (SD4, SD12, SD22),[19] and the ultrapotent ZS1C5[50]. Like BD70-4003, the JK series and SD series primarily target Domain I. SD4 and SD22 exhibit picomolar binding affinities (32–83 pM) and have shown 100% protection in mice when given at 20 mg/kg at 3 dpi, representing a potentially wider therapeutic window than the BD70 series if higher doses are used.

The antibody ZS1C5 represents a distinct class of "interdomain" neutralizers.[50] Structural analysis has revealed that ZS1C5 bridges Domain I and Domain III of the Gn-head, mediated by an unusually long CDRH3 of over 17 residues. ZS1C5 exhibits subnanomolar potency and has demonstrated robust protection in both murine and non-human primate (NHP) models, the latter being a significant milestone for SFTSV therapeutics. While BD70-4003 and BD70-4017 target more traditional domain-specific epitopes, their high efficacy and distinct binding sites make them excellent partners for cocktails, potentially mirroring the success seen with other emerging interdomain-targeting platforms.

In conclusion, the delineation of the SFTSV Gn antigenic landscape and the functional

299 characterization of human mAbs provides a definitive path forward for both therapy and prevention.
300 The integration of high-throughput mutational screening with atomic-level structural analysis has
301 resolved long-standing questions regarding epitope-function relationships, identifying the Gn-head
302 Domain I and Domain III as the primary targets for neutralizing intervention. The unique structural
303 insights provided by the DMS-cryo-EM synergy not only advance the development of SFTSV-
304 specific drugs but also establish a generalizable model for responding to other emerging tick-borne
305 viruses. These findings, coupled with the demonstration of 100% in vivo protection, provide a robust
306 foundation for the rational design of universal vaccines for SFTSV and its related pathogens.

307 **Limitations of the study**

308 Our study has established a powerful framework for discovering bunyavirus antibodies by
309 employing DMS and identified promising therapeutic candidates, but some limitations remain. First,
310 the binding sites of some mAbs cannot be efficiently identified by DMS due to weak escape signal
311 or high noise from non-epitope sites, and the DMS-based unsupervised clustering is limited by the
312 size of mAb collection in this study. These epitope mapping results could be complemented by
313 structural analyses. Second, the conclusions derived from pseudovirus-based neutralization assays
314 cannot be always directly translated to inhibition against live-virus or efficacy *in vivo*, highlighting
315 the necessity of further validation. Lastly, the effectiveness of BD70-4003 or BD70-4017 against
316 advanced-stage infections has not been fully demonstrated, since patients typically present for
317 treatment multiple days after symptoms emerge. Further pre-clinical and clinical research should
318 prioritize refining dosing protocols and assessing long-term safety and efficacy.
319

320 **RESOURCE AVAILABILITY**

321 **Lead contact**

322 Further information and requests for resources and reagents should be directed to and will be
323 fulfilled by the lead contact, yunlongcao@pku.edu.cn (Y.C.).
324

325 **Materials availability**

326 All unique reagents generated in this study are available from the lead contact with a completed
327 Material Transfer Agreement.

Data and code availability

All data and materials presented in this manuscript are available from the lead contact upon a reasonable request under a completed Material Transfer Agreement. This paper does not report original code. Any additional information required to reanalyze the data reported in this paper is available from the lead contact upon request.

ACKNOWLEDGMENTS

We thank Yantai Qishan Hospital for the assistance in recruiting SFTSV-infected convalescents and collecting samples. We thank Yuhang Wang from Changping Laboratory for the support of structure analysis. We thank Nanjing GenScript Biotechnology for the technical assistance on the purification of mAbs. This project is financially supported by Changping Laboratory (2025D-04-01).

AUTHOR CONTRIBUTIONS

Y.C. designed the study. Y.C., Q.W., and J.L. wrote the manuscript with input from all authors. Y.C. and F.S. coordinated the expression and characterization of the neutralizing antibodies. F.J., Q.W., and H.S. performed and analyzed the yeast display screening experiments. Q.W., Y.Y., J.W., L.Y., and Y.W. performed the neutralizing antibody expression and characterization, including pseudovirus neutralization assays and ELISA. Q.W., M.M, and F.J. performed and analyzed the antigen-specific single B cell VDJ sequencing. Y.W. and Q.W. performed the structural analyses. W.L., H.L. and A.H. performed and coordinated the authentic virus neutralization and animal experiments. Y.L. and L.Z. recruited the SFTSV convalescents.

DECLARATION OF INTERESTS

Provisional patents related to the antibodies identified in this paper have been filed. Y.C. is the co-founder of Singlomics Biopharmaceuticals.

SUPPLEMENTAL INFORMATION

Document S1. Figures S1–S6, Tables S1–S8

FIGURE TITLES AND LEGENDS

357 **Figure 1. Identification of broad neutralizing antibodies from SFTSV-infected convalescents**

358 (A) The median effective dose (ED_{50}) of plasma from SFTSV-infected convalescents was
359 determined by ELISA. The average value of each group was marked.

360 (B) The half maximal neutralization titre (NT_{50}) of plasma against VSV-based SFTSV
361 pseudoviruses.

362 (C-D) Neutralizing median inhibition concentration (IC_{50}, μg/ml) of SFTSV Gn (C) or Gc (D)
363 antibodies using VSV-based pseudoviruses. Neutralization assays were conducted in at least two
364 biological replicates.

365

366 **Figure 2. Epitope analysis of all Gn antibodies by yeast DMS**

367 (A) Structural schematic of SFTSV Gn-head. The left panel illustrates the delineation of the three
368 domains, colored in blue-white (I), pale cyan (II), and gray (III), respectively; the corresponding
369 structural schematic is shown in the right panel (PDB: 5Y10).

370 (B) Structural projections and key epitope annotations of the eight DMS groups with different colors.
371 The region outlined by the curved line corresponds to the epitope of each respective group. In the
372 structural projection, amino acid residues with higher DMS scores are displayed in darker colors.

373 (C) Average escape scores of antibodies in eight groups. Colors are assigned according to the type
374 of amino acids, and the heights of the letters in the logo plot indicate escape scores. Residues are
375 numbered based on Gn-head numbering.

376 (D) The gene analysis of the antibodies in eight groups. Sankey diagram was generated to visualize
377 the correspondence between heavy and light chains for the antibody genes in each group, with
378 asterisks indicating the inclusion of control antibodies.

379 (E-F) Statistical analysis of the number (E) and IC_{50} values (mean SEM) (F) for neutralization
380 against the HB29 strain across DMS-classified antibody groups was performed.

381

382 **Figure 3. MAb-mediated protection of authentic virus challenge *in vitro* and *in vivo***

383 (A-B) The neutralization activity of six selected mAbs against four SFTSV authentic virus. The
384 $FRNT_{50}$ was calculated using the equation of log [inhibitor] versus response-variable slope (four
385 parameters) method. Data were shown as mean SD values from three biologically independent
386 replicates.

387 (C and F) Schematic of the design for the HBMC16 challenge experiment in mice. In prophylactic
388 groups (C), 5 mg/kg mAb was administered intraperitoneally and challenged by HBMC16
389 intraperitoneally 1 day later (C). In therapeutic groups (F), antibodies were given intraperitoneally
390 1 day after virus challenge. Each group consists of 6 mice.

391 (D and G) Survival curves of mice in each group.

392 (E, H and I) Viral load in the serum of mice in each group.

393 (J-L) Viral load (mean SD) of mice challenged by HBMC16 in spleen (J), liver (K), or lung (L).
394 Each point corresponds to samples from a mouse. The limit of detection is about 1.81×10^2 copies/g
395 and is shown as the dashed line.

396

397 **Figure 4. Cryo-EM structure of Gn antibodies bound to HB29-Gn-head**

398 (A, D, G and J) Aligned structures of BD70-4003 (A), BD70-4003/BD70-4017 (D), BD70-4008 (G)
399 and BD70-4008/BD70-4017 (J) on SFTSV Gn-head. BD70-4003, BD70-4008 and BD70-4017 are
400 colored in blue, orange, and green, respectively. Gn-head is colored in gray.

401 (B, E and H) Surface representation of the contact residues on Gn-head interacting with BD70-4003
402 (B), BD70-4017 (E) and BD70-4008 (H).

403 (C, F and I) Interactions between the heavy-chain and light-chain BD70-4003 (C), BD70-4017 (F)
404 and BD70-4008 (I) and Gn-head. Residues of Gn-head, BD70-4003, BD70-4008 or BD70-4017 are
405 gray, blue, orange, and green, respectively.

406 (K) The overlapping epitopes of BD70-4008 and BD70-4017 are labeled in purple.

407

408 **Figure 5. Docking of three antibodies onto the surface of the SFTSV virion**

409 Docking of BD70-4003/BD70-4017 (A) and BD70-4008/BD70-4017 (B) onto the surface of
410 SFTSV virion (PDB: 8I4T). BD70-4003, BD70-4008 and BD70-4017 are colored in blue, orange,
411 and green, respectively. The binding sites of mAbs on SFTSV virion are labeled with colors within
412 the same palette.

413

414 **REFERENCES**

415 1. Yu, X.J., Liang, M.F., Zhang, S.Y., Liu, Y., Li, J.D., Sun, Y.L., Zhang, L., Zhang, Q.F., Popov,
416 V.L., Li, C., et al. (2011). Fever with thrombocytopenia associated with a novel bunyavirus in
417 China. N Engl J Med *364*, 1523-1532. 10.1056/NEJMoa1010095.
418 2. Liu, W., Lu, Q.B., Cui, N., Li, H., Wang, L.Y., Liu, K., Yang, Z.D., Wang, B.J., Wang, H.Y.,
419 Zhang, Y.Y., et al. (2013). Case-fatality ratio and effectiveness of ribavirin therapy among
420 hospitalized patients in china who had severe fever with thrombocytopenia syndrome. Clin
421 Infect Dis *57*, 1292-1299. 10.1093/cid/cit530.
422 3. Liu, Q., He, B., Huang, S.Y., Wei, F., and Zhu, X.Q. (2014). Severe fever with thrombocytopenia
423 syndrome, an emerging tick-borne zoonosis. Lancet Infect Dis *14*, 763-772. 10.1016/S1473-
424 3099(14)70718-2.
425 4. Yang, T., Huang, H., Jiang, L., and Li, J. (2022). Overview of the immunological mechanism
426 underlying severe fever with thrombocytopenia syndrome (Review). Int J Mol Med *50*.
427 10.3892/ijmm.2022.5174.
428 5. Wang, Y., Song, Z., Wei, X., Yuan, H., Xu, X., Liang, H., and Wen, H. (2022). Clinical laboratory
429 parameters and fatality of Severe fever with thrombocytopenia syndrome patients: A systematic
430 review and meta-analysis. PLoS Negl Trop Dis *16*, e0010489. 10.1371/journal.pntd.0010489.
431 6. Li, H., Lu, Q.-B., Xing, B., Zhang, S.-F., Liu, K., Du, J., Li, X.-K., Cui, N., Yang, Z.-D., Wang,
432 L.-Y., et al. (2018). Epidemiological and clinical features of laboratory-diagnosed severe fever

with thrombocytopenia syndrome in China, 2011–17: a prospective observational study. The Lancet Infectious Diseases *18*, 1127-1137. 10.1016/s1473-3099(18)30293-7.

7. Egizi, A., Bulaga-Seraphin, L., Alt, E., Bajwa, W.I., Bernick, J., Bickerton, M., Campbell, S.R., Connally, N., Doi, K., Falco, R.C., et al. (2020). First glimpse into the origin and spread of the Asian longhorned tick, Haemaphysalis longicornis, in the United States. Zoonoses Public Health *67*, 637-650. 10.1111/zph.12743.

8. Miao, D., Dai, K., Zhao, G.P., Li, X.L., Shi, W.Q., Zhang, J.S., Yang, Y., Liu, W., and Fang, L.Q. (2020). Mapping the global potential transmission hotspots for severe fever with thrombocytopenia syndrome by machine learning methods. Emerg Microbes Infect *9*, 817-826. 10.1080/22221751.2020.1748521.

9. Zhang, X., Zhao, C., Cheng, C., Zhang, G., Yu, T., Lawrence, K., Li, H., Sun, J., Yang, Z., Ye, L., et al. (2022). Rapid Spread of Severe Fever with Thrombocytopenia Syndrome Virus by Parthenogenetic Asian Longhorned Ticks. Emerg Infect Dis *28*, 363-372. 10.3201/eid2802.211532.

10. Spiegel, M., Plegge, T., and Pohlmann, S. (2016). The Role of Phlebovirus Glycoproteins in Viral Entry, Assembly and Release. Viruses *8*. 10.3390/v8070202.

11. Halldorsson, S., Behrens, A.J., Harlos, K., Huiskonen, J.T., Elliott, R.M., Crispin, M., Brennan, B., and Bowden, T.A. (2016). Structure of a phleboviral envelope glycoprotein reveals a consolidated model of membrane fusion. Proc Natl Acad Sci U S A *113*, 7154-7159. 10.1073/pnas.1603827113.

12. Du, S., Peng, R., Xu, W., Qu, X., Wang, Y., Wang, J., Li, L., Tian, M., Guan, Y., Wang, J., et al. (2023). Cryo-EM structure of severe fever with thrombocytopenia syndrome virus. Nat Commun *14*, 6333. 10.1038/s41467-023-41804-7.

13. Wu, Y., Zhu, Y., Gao, F., Jiao, Y., Oladejo, B.O., Chai, Y., Bi, Y., Lu, S., Dong, M., Zhang, C., et al. (2017). Structures of phlebovirus glycoprotein Gn and identification of a neutralizing antibody epitope. Proc Natl Acad Sci U S A *114*, E7564-E7573. 10.1073/pnas.1705176114.

14. Kim, K.H., Kim, J., Ko, M., Chun, J.Y., Kim, H., Kim, S., Min, J.Y., Park, W.B., Oh, M.D., and Chung, J. (2019). An anti-Gn glycoprotein antibody from a convalescent patient potently inhibits the infection of severe fever with thrombocytopenia syndrome virus. PLoS Pathog *15*, e1007375. 10.1371/journal.ppat.1007375.

15. Ren, X., Sun, J., Kuang, W., Yu, F., Wang, B., Wang, Y., Deng, W., Xu, Z., Yang, S., Wang, H., et al. (2024). A broadly protective antibody targeting glycoprotein Gn inhibits severe fever with thrombocytopenia syndrome virus infection. Nat Commun *15*, 7009. 10.1038/s41467-024-51108-z.

16. Yang, P., Wu, X., Shang, H., Sun, Z., Wang, Z., Song, Z., Yuan, H., Deng, F., Shen, S., Guo, Y., and Zhang, N. (2024). Molecular mechanism and structure-guided humanization of a broadly neutralizing antibody against SFTSV. PLoS Pathog *20*, e1012550. 10.1371/journal.ppat.1012550.

17. Wu, X., Moming, A., Zhang, Y., Wang, Z., Zhang, T., Fu, L., Qian, J., Ni, J., Hu, S., Tang, S., et al. (2024). Identification and characterization of three monoclonal antibodies targeting the SFTSV glycoprotein and displaying a broad spectrum recognition of SFTSV-related viruses. PLoS Negl Trop Dis *18*, e0012216. 10.1371/journal.pntd.0012216.

18. Zhang, S., Shang, H., Han, S., Li, J., Peng, X., Wu, Y., Yang, X., Leng, Y., Wang, F., Cui, N., et al. (2025). Discovery and characterization of potent broadly neutralizing antibodies from human

survivors of severe fever with thrombocytopenia syndrome. EBioMedicine *111*, 105481. 10.1016/j.ebiom.2024.105481.

19. Quan, C., Nie, K., Ma, D., Su, C., Li, L., Zheng, W., Yin, C., Wang, Y., Yang, P., Peng, D., et al. (2025). Molecular mechanism of potently neutralizing human monoclonal antibodies against severe fever with thrombocytopenia virus infection. J Virol *99*, e0053325. 10.1128/jvi.00533-25.

20. Greaney, A.J., Starr, T.N., Gilchuk, P., Zost, S.J., Binshtein, E., Loes, A.N., Hilton, S.K., Huddleston, J., Eguia, R., Crawford, K.H.D., et al. (2021). Complete Mapping of Mutations to the SARS-CoV-2 Spike Receptor-Binding Domain that Escape Antibody Recognition. Cell Host Microbe *29*, 44-57 e49. 10.1016/j.chom.2020.11.007.

21. Cao, Y., Wang, J., Jian, F., Xiao, T., Song, W., Yisimayi, A., Huang, W., Li, Q., Wang, P., An, R., et al. (2022). Omicron escapes the majority of existing SARS-CoV-2 neutralizing antibodies. Nature *602*, 657-663. 10.1038/s41586-021-04385-3.

22. Jian, F., Wang, J., Yisimayi, A., Song, W., Xu, Y., Chen, X., Niu, X., Yang, S., Yu, Y., Wang, P., et al. (2025). Evolving antibody response to SARS-CoV-2 antigenic shift from XBB to JN.1. Nature *637*, 921-929. 10.1038/s41586-024-08315-x.

23. Yisimayi, A., Song, W., Wang, J., Jian, F., Yu, Y., Chen, X., Xu, Y., Yang, S., Niu, X., Xiao, T., et al. (2024). Repeated Omicron exposures override ancestral SARS-CoV-2 immune imprinting. Nature *625*, 148-156. 10.1038/s41586-023-06753-7.

24. Cao, Y., Jian, F., Wang, J., Yu, Y., Song, W., Yisimayi, A., Wang, J., An, R., Chen, X., Zhang, N., et al. (2023). Imprinted SARS-CoV-2 humoral immunity induces convergent Omicron RBD evolution. Nature *614*, 521-529. 10.1038/s41586-022-05644-7.

25. Cao, Y., Yisimayi, A., Jian, F., Song, W., Xiao, T., Wang, L., Du, S., Wang, J., Li, Q., Chen, X., et al. (2022). BA.2.12.1, BA.4 and BA.5 escape antibodies elicited by Omicron infection. Nature *608*, 593-602. 10.1038/s41586-022-04980-y.

26. Cao, Y., Jian, F., Zhang, Z., Yisimayi, A., Hao, X., Bao, L., Yuan, F., Yu, Y., Du, S., Wang, J., et al. (2022). Rational identification of potent and broad sarbecovirus-neutralizing antibody cocktails from SARS convalescents. Cell Rep *41*, 111845. 10.1016/j.celrep.2022.111845.

27. Jian, F., Wec, A.Z., Feng, L., Yu, Y., Wang, L., Wang, P., Yu, L., Wang, J., Hou, J., Berrueta, D.M., et al. (2025). Viral evolution prediction identifies broadly neutralizing antibodies to existing and prospective SARS-CoV-2 variants. Nat Microbiol *10*, 2003-2017. 10.1038/s41564-025-02030-7.

28. Chung, H., Kim, E., Kwon, B., Cho, Y.G., Bae, S., Jung, J., Kim, M.J., Chong, Y.P., Kim, S.H., Lee, S.O., et al. (2022). Kinetics of Glycoprotein-Specific Antibody Response in Patients with Severe Fever with Thrombocytopenia Syndrome. Viruses *14*. 10.3390/v14020256.

29. Li, J.C., Ding, H., Wang, G., Zhang, S., Yang, X., Wu, Y.X., Peng, X.F., Zhang, X.A., Yang, Z.D., Cui, N., et al. (2023). Dynamics of neutralizing antibodies against severe fever with thrombocytopenia syndrome virus. Int J Infect Dis *134*, 95-98. 10.1016/j.ijid.2023.05.018.

30. Fu, Y., Li, S., Zhang, Z., Man, S., Li, X., Zhang, W., Zhang, C., and Cheng, X. (2016). Phylogeographic analysis of severe fever with thrombocytopenia syndrome virus from Zhoushan Islands, China: implication for transmission across the ocean. Sci Rep *6*, 19563. 10.1038/srep19563.

31. Yun, S.M., Park, S.J., Park, S.W., Choi, W., Jeong, H.W., Choi, Y.K., and Lee, W.J. (2017). Molecular genomic characterization of tick- and human-derived severe fever with

521 thrombocytopenia syndrome virus isolates from South Korea. PLoS Negl Trop Dis *11*,
522 e0005893. 10.1371/journal.pntd.0005893.
523 32. Xu, J., Liu, Y., Zhang, F., Wang, X., Huang, W., Wu, Y., Li, B., Zhuang, J., Bing, Y., Wang, Y.,
524 and Qiao, Y. (2022). Analysis of cross neutralizing activity of antibodies from sera of severe
525 fever with thrombocytopenia syndrome patients to deal with different genotype strains. Front
526 Microbiol *13*, 1020545. 10.3389/fmicb.2022.1020545.
527 33. Guo, X., Zhang, L., Zhang, W., Chi, Y., Zeng, X., Li, X., Qi, X., Jin, Q., Zhang, X., Huang, M.,
528 et al. (2013). Human antibody neutralizes severe Fever with thrombocytopenia syndrome virus,
529 an emerging hemorrhagic Fever virus. Clin Vaccine Immunol *20*, 1426-1432.
530 10.1128/CVI.00222-13.
531 34. Park, S.Y., Choi, W., Chong, Y.P., Park, S.W., Wang, E.B., Lee, W.J., Jee, Y., Kwon, S.W., and
532 Kim, S.H. (2016). Use of Plasma Therapy for Severe Fever with Thrombocytopenia Syndrome
533 Encephalopathy. Emerg Infect Dis *22*, 1306-1308. 10.3201/eid2207.151791.
534 35. Choi, S., Kim, M.C., Kwon, J.S., Kim, J.Y., Lee, K.H., and Kim, S.H. (2018). Case Report: Use
535 of Plasma Exchange Followed by Convalescent Plasma Therapy in a Critically Ill Patient with
536 Severe Fever and Thrombocytopenia Syndrome-Associated Encephalopathy:
537 Cytokine/Chemokine Concentrations, Viral Loads, and Antibody Responses. Am J Trop Med
538 Hyg *99*, 1466-1468. 10.4269/ajtmh.17-0766.
539 36. Starr, T.N., Greaney, A.J., Addetia, A., Hannon, W.W., Choudhary, M.C., Dingens, A.S., Li, J.Z.,
540 and Bloom, J.D. (2021). Prospective mapping of viral mutations that escape antibodies used to
541 treat COVID-19. Science *371*, 850-854. 10.1126/science.abf9302.
542 37. Starr, T.N., Greaney, A.J., Dingens, A.S., and Bloom, J.D. (2021). Complete map of SARS-
543 CoV-2 RBD mutations that escape the monoclonal antibody LY-CoV555 and its cocktail with
544 LY-CoV016. Cell Rep Med *2*, 100255. 10.1016/j.xcrm.2021.100255.
545 38. Sivelle, C., Sierocki, R., Lesparre, Y., Lomet, A., Quintilio, W., Dubois, S., Correia, E., Moro,
546 A.M., Maillere, B., and Nozach, H. (2023). Combining deep mutational scanning to heatmap of
547 HLA class II binding of immunogenic sequences to preserve functionality and mitigate
548 predicted immunogenicity. Front Immunol *14*, 1197919. 10.3389/fimmu.2023.1197919.
549 39. Chang, Z., Gao, D., Liao, L., Sun, J., Zhang, G., Zhang, X., Wang, F., Li, C., Oladejo, B.O., Li,
550 S., et al. (2024). Bispecific antibodies targeting two glycoproteins on SFTSV exhibit synergistic
551 neutralization and protection in a mouse model. Proc Natl Acad Sci U S A *121*, e2400163121.
552 10.1073/pnas.2400163121.
553 40. Zhang, L., Peng, X., Wang, Q., Li, J., Lv, S., Han, S., Zhang, L., Ding, H., Wang, C., Xiao, G.,
554 et al. (2023). CCR2 is a host entry receptor for severe fever with thrombocytopenia syndrome
555 virus. Science Advances *9*, eadg6856. 10.1126/sciadv.adg6856.
556 41. Wang, L., Wang, J., Zhang, J., Wang, X., Cao, W., Yang, L., Wu, Y., Li, B., and Qiao, Y. (2025).
557 Weakened invasion of severe fever with thrombocytopenia syndrome bunyavirus beneficial to
558 its immune escape by multi-site mutation of glycoprotein. Molecular Genetics and Genomics
559 *300*. 10.1007/s00438-025-02319-6.
560 42. Sun, Z., Cheng, J., Bai, Y., Cao, L., Xie, D., Deng, F., Zhang, X., Rao, Z., and Lou, Z. (2023).
561 Architecture of severe fever with thrombocytopenia syndrome virus. Protein Cell *14*, 914-918.
562 10.1093/procel/pwad019.
563 43. Zhai, Y., Li, H., Xia, P., Jiang, Y., Tong, H., Zhou, D., Jiang, C., Liu, Y., and Wang, J. (2024).
564 Intravenous immunoglobulin-based adjuvant therapy for severe fever with thrombocytopenia

565 syndrome: A single-center retrospective cohort study. J Med Virol *96*, e70017.
566 10.1002/jmv.70017.
567 44. Song, X., Xu, X., Ren, X., Ruan, X., and Bo, J. (2024). Therapeutic plasma exchange combined
568 with ribavirin to rescue critical SFTS patients. J Clin Apher *39*, e22131. 10.1002/jca.22131.
569 45. Wang, W., Zhang, A., Wu, Q., Zhu, L., and Yang, J. (2022). Epidemiological and Clinical
570 Characteristics of Severe Fever with Thrombocytopenia Syndrome in Southern Anhui Province,
571 China, 2011-2020. Jpn J Infect Dis *75*, 133-139. 10.7883/yoken.JJID.2021.391.
572 46. Zu, Z., Hu, Y., Zheng, X., Chen, C., Zhao, Y., Jin, Y., Lin, H., and He, N. (2022). A ten-year
573 assessment of the epidemiological features and fatal risk factors of hospitalised severe fever
574 with thrombocytopenia syndrome in Eastern China. Epidemiol Infect *150*, e131.
575 10.1017/S0950268822001108.
576 47. Engdahl, T.B., Binshtein, E., Brocato, R.L., Kuzmina, N.A., Principe, L.M., Kwilas, S.A., Kim,
577 R.K., Chapman, N.S., Porter, M.S., Guardado-Calvo, P., et al. (2023). Antigenic mapping and
578 functional characterization of human New World hantavirus neutralizing antibodies. Elife *12*.
579 10.7554/eLife.81743.
580 48. Hofmann, H., Li, X., Zhang, X., Liu, W., Kuhl, A., Kaup, F., Soldan, S.S., Gonzalez-Scarano,
581 F., Weber, F., He, Y., and Pohlmann, S. (2013). Severe fever with thrombocytopenia virus
582 glycoproteins are targeted by neutralizing antibodies and can use DC-SIGN as a receptor for
583 pH-dependent entry into human and animal cell lines. J Virol *87*, 4384-4394.
584 10.1128/JVI.02628-12.
585 49. Chen, R., Huang, W., and Wang, Y. (2023). Pseudotyped Virus for Bandavirus. Adv Exp Med
586 Biol *1407*, 265-277. 10.1007/978-981-99-0113-5_14.
587 50. Bi, J., Dai, Z., Hong, X., Zhang, Y., Lu, S., Wang, Q., Liu, Y., Li, X., Li, M., Song, G., et al.
588 (2026). A potent interdomain epitope-targeting antibody protects against SFTSV in mice and
589 non-human primates. Vita. 10.15302/vita.2025.12.0002.
590 51. Gietz, R.D., and Schiestl, R.H. (2007). High-efficiency yeast transformation using the LiAc/SS
591 carrier DNA/PEG method. Nat Protoc *2*, 31-34. 10.1038/nprot.2007.13.
592 52. Du, S., Cao, Y., Zhu, Q., Yu, P., Qi, F., Wang, G., Du, X., Bao, L., Deng, W., Zhu, H., et al.
593 (2020). Structurally Resolved SARS-CoV-2 Antibody Shows High Efficacy in Severely
594 Infected Hamsters and Provides a Potent Cocktail Pairing Strategy. Cell *183*, 1013-1023 e1013.
595 10.1016/j.cell.2020.09.035.
596 53. Du, S., Liu, P., Zhang, Z., Xiao, T., Yasimayi, A., Huang, W., Wang, Y., Cao, Y., Xie, X.S., and
597 Xiao, J. (2021). Structures of SARS-CoV-2 B.1.351 neutralizing antibodies provide insights
598 into cocktail design against concerning variants. Cell Res *31*, 1130-1133. 10.1038/s41422-021-
599 00555-0.
600 54. Punjani, A., Rubinstein, J.L., Fleet, D.J., and Brubaker, M.A. (2017). cryoSPARC: algorithms
601 for rapid unsupervised cryo-EM structure determination. Nat Methods *14*, 290-296.
602 10.1038/nmeth.4169.
603 55. Pettersen, E.F., Goddard, T.D., Huang, C.C., Couch, G.S., Greenblatt, D.M., Meng, E.C., and
604 Ferrin, T.E. (2004). UCSF Chimera--a visualization system for exploratory research and
605 analysis. J Comput Chem *25*, 1605-1612. 10.1002/jcc.20084.
606 56. Emsley, P., Lohkamp, B., Scott, W.G., and Cowtan, K. (2010). Features and development of
607 Coot. Acta Crystallogr D Biol Crystallogr *66*, 486-501. 10.1107/S0907444910007493.
608 57. Liebschner, D., Afonine, P.V., Baker, M.L., Bunkoczi, G., Chen, V.B., Croll, T.I., Hintze, B.,

609 Hung, L.W., Jain, S., McCoy, A.J., et al. (2019). Macromolecular structure determination using
610 X-rays, neutrons and electrons: recent developments in Phenix. Acta Crystallogr D Struct Biol
611 *75*, 861-877. 10.1107/S2059798319011471.
612 58. Pettersen, E.F., Goddard, T.D., Huang, C.C., Meng, E.C., Couch, G.S., Croll, T.I., Morris, J.H.,
613 and Ferrin, T.E. (2021). UCSF ChimeraX: Structure visualization for researchers, educators,
614 and developers. Protein Sci *30*, 70-82. 10.1002/pro.3943.
615

616 **METHOD DETAILS**

617 **Plasma donors**

618 Blood samples were collected from 12 convalescent individuals previously infected with SFTSV.
619 All plasma-related experiments were approved by the Ethics Committee of Beijing Ditan Hospital,
620 Capital Medical University (approval no. DTEC-KY2022-022-01). Written informed consent was
621 obtained from all participants in accordance with the Declaration of Helsinki, permitting the
622 collection, storage, and research use of clinical samples, as well as publication of resulting data.

623 Whole blood samples were diluted 1:1 with PBS containing 2% FBS and subjected to Ficoll (Cytiva,
624 17-1440-03) density gradient centrifugation to separate plasma and PBMCs. Plasma was collected
625 from the upper layer, while cells at the interface were harvested for PBMC isolation. PBMCs were
626 further processed by centrifugation, red blood cell lysis (Invitrogen eBioscience 1× RBC Lysis
627 Buffer, 00-4333-57), and washing steps. Samples not used immediately were were stored in FBS
628 (Gibco) containing 10% DMSO (Sigma) in liquid nitrogen. Cryopreserved PBMCs were thawed in
629 DPBS containing 2% FBS (Stemcell, 07905) prior to use.

630 **Antigen-specific cell sorting, V(D)J sequencing, and data analysis**

631 PBMCs were processed using the EasySep Human CD19 Positive Selection Kit II (STEMCELL,
632 17854) to isolate $CD19^{+}$ B cells. Cells were stained with FITC anti-human CD19 (BioLegend,
633 302206, clone HIB19), Brilliant Violet 421 anti-human CD27 (BioLegend, 302824, clone O323),
634 and PE/Cyanine7 anti-human IgM (BioLegend, 314532, clone MHM-88). For antigen labeling,
635 biotinylated SFTSV HB29-Gn or HB29-Gc protein was conjugated with PE-streptavidin
636 (BioLegend, 405204) and APC-streptavidin (BioLegend, 405207), respectively. Biotinylated
637 ovalbumin (OVA) conjugated with streptavidin served as a negative control. Specifically, HB29-Gn
638 and HB29-Gc were labeled with distinct barcodes: Gn was conjugated with TotalSeq™-C0971 and
639 TotalSeq™-C0972 Streptavidin (BioLegend, 405271 and 405273), while Gc was conjugated with

640 TotalSeq™-C0973 and TotalSeq™-C0974 Streptavidin (BioLegend, 405275 and 405277) to enable
641 sequencing-adapted sorting. OVA was labeled with TotalSeq™-C0975 Streptavidin (BioLegend,
642 405279). Cells were incubated on ice in the dark for 30 minutes and washed twice. Dead cells were
643 excluded by 7-AAD staining (Invitrogen, 00-6993-50). 7-AAD^{-}, CD19^{+}, CD27^{+}, IgM^{-}, OVA^{-}, and
644 antigen-positive (Gn^{+} or Gc^{+}) B cells were sorted using a MoFlo Astrios EQ Cell Sorter (Beckman
645 Coulter). FACS data were acquired with Summit 6.0 (Beckman Coulter) and analyzed using FlowJo
646 v10.8 (BD Biosciences).

647 Sorted cells were processed using the 10X Genomics Chromium Next GEM Single Cell V(D)J kit
648 (v1.1, CG000208) according to the manufacturer's protocol to generate barcoded libraries via GEM
649 formation, reverse transcription, and cDNA amplification. Libraries were sequenced on an Illumina
650 platform.

651 BCR contigs were assembled and aligned to the reference using Cell Ranger (v6.1.1). Only
652 productive contigs and B cells with paired heavy and light chains were retained after quality filtering.
653 Germline V(D)J gene annotation was performed with IgBlast (v1.17.1), and somatic hypermutations
654 were analyzed using the Change-O toolkit (v1.2.0).

655 **Monoclonal antibody expression and purification**

656 Human antibody heavy- and light-chain genes were synthesized and cloned into respective pCMV3
657 vectors (pCMV3-CH, pCMV3-CL, or pCMV3-CK). Following transformation into E. coli DH5α
658 (Tsingke, TSC-C01-96) and overnight incubation at 37°C, positive clones were identified by colony
659 PCR and Sanger sequencing, followed by plasmid preparation (CWBIO, CW2105). For protein
660 expression, Expi293F cells were co-transfected with paired plasmids using polyethylenimine
661 (Yeasen, 40816ES03) in 0.9% NaCl. Transfected cultures were maintained under standard growth
662 conditions, with nutrient supplement (OPM Biosciences, F081918-001) added 24 h post-
663 transfection and replenished every 48 h. Supernatants were harvested after 8 days of culture for
664 antibody purification.

665 Antibodies were purified from clarified supernatant (3,000 × g, 10 min) using Protein A magnetic
666 beads (GenScript, L00695) and a KingFisher system (Thermo Fisher). Final samples were

667 quantified by NanoDrop (Thermo Fisher, 840-317400) and analyzed for purity by SDS-PAGE
668 (LabLead, P42015).

669 **ELISA**

670 Purified SFTSV Gn or Gc proteins (1 μg/mL in Solarbio C1055 buffer) were used to coat ELISA
671 plates overnight at 4°C. After washing and blocking, serially diluted antibodies were added and
672 incubated for 30 minutes at room temperature. The plates were then incubated with an HRP-
673 conjugated goat anti-human IgG (Jackson ImmunoResearch, 109-035-003; 0.25 μg/mL) for 30
674 minutes, followed by tetramethylbenzidine (TMB) substrate (Solarbio, PR1200) for signal
675 development. The reaction was terminated with H_2SO_4, and absorbance at 450 nm was read on a
676 microplate reader (Multiskan Fc, Thermo Scientific).

677 **Surface Plasmon Resonance**

678 SPR experiments were performed on a Biacore 8K (Cytiva). SFTSV mAbs (human IgG1) were
679 captured by a Sensor Chip Protein A (Cytiva). Various concentrations of SFTSV Gn (His-tag; 1.5625,
680 6.25, 12.5, 25, and 50 nM) were injected. The response was recorded at room temperature, and the
681 raw data curves were fitted to a 1:1 binding model using Biacore Insight Evaluation Software
682 (Cytiva, v4.0.8).

683 **Pseudovirus neutralization assay**

684 SFTSV Gn/Gc pseudoviruses were produced using a VSV-based system. Briefly, 293T cells were
685 infected with G*ΔG-VSV (Kerafast) and transfected with a plasmid encoding the SFTSV
686 glycoproteins. The culture supernatant containing the pseudoviruses was collected, clarified by
687 filtration, aliquoted, and stored at -80°C. For the neutralization assay, serially diluted monoclonal
688 antibodies were mixed with pseudoviruses and incubated for 1 hour at 37°C with 5% CO_2. Huh-7
689 cells were then added to the mixture. After 48 hours, the supernatant was removed, and
690 luminescence was measured following the addition of D-luciferin substrate (PerkinElmer, 6066769)
691 using a microplate reader (PerkinElmer, HH3400). The half-maximal inhibitory concentration (IC_{50})
692 was determined by fitting the data to a four-parameter logistic model in GraphPad Prism (v9.0.1).

693 **DMS library construction**

694 DMS libraries were constructed as previously described, with modifications for the SFTSV Gn-
695 head domain (residues 20-340). Using the HB29 Gn-head coding sequence as a template, two
696 independent mutant libraries were generated via three rounds of mutagenesis PCR with synthesized
697 primer pools. Each Gn-head variant was constructed with an N-terminal HA tag and a C-terminal
698 MYC tag, linked to a unique 26-nucleotide barcode. Barcode-variant mapping was performed by
699 PacBio sequencing. The mutant libraries were cloned into the pETcon vector and electroporated into
700 DH10B cells for plasmid amplification. Plasmids were then transformed into the EBY100 strain of
701 Saccharomyces cerevisiae as previously reported.[51] Transformed yeast were selected on SD-CAA
702 plates and expanded in SD-CAA liquid medium. Yeast libraries were flash-frozen in liquid nitrogen
703 and stored at -80°C.

704 **High-throughput antibody-escape profiling**

705 Antibody escape mutations were assessed using a FACS-based workflow. Yeast-expressing Gn-head
706 mutants were induced overnight and stained. After incubation with primary Gn mAbs for 30 minutes
707 at 4°C, cells were stained with secondary antibodies: APC anti-HA.11 (BioLegend, 901524), FITC-
708 conjugated chicken anti-c-Myc (icllab, CMYC-45F), and PE-conjugated goat anti-human IgG
709 (Jackson, 109-115-098) for 30 minutes at 4°C. Double-positive (MYC^+ HA^+) yeast displaying
710 bound mAbs were gated, and mAb-unbound populations adjacent to the main population were
711 sorted and collected. Plasmid DNA was extracted after 40 hours of culture, barcodes were PCR-
712 amplified, purified with AMPure XP beads (Beckman Coulter, A63882), and subjected to high-
713 throughput sequencing on an Illumina NovaSeq X Plus platform.

714 **Processing of DMS data**

715 Illumina single-end sequencing reads from Gn-head DMS libraries were processed as described
716 with minor modifications. Raw reads were trimmed to 26 bp and mapped to a barcode-variant
717 dictionary using the dms_variants package (v0.8.9). Variant escape scores were calculated as
718 $F \times (n_{X,ab}/N_{ab})/(n_{X,ref}/N_{ref})$, where $n_{X,ab}$ and $n_{X,ref}$ is the number of reads representing variant X, and
719 N_{ab} and N_{ref} are the total number of valid reads in antibody-selected (ab) and reference (ref) library,
720 respectively. F is a normalization factor defined as the 99th percentile of escape fraction ratios.
721 Variants with fewer than six reads in the reference library or those associated with severely impaired

722 Gn-head expression were excluded. Global epistasis models were fitted using dms_variants to infer
723 per-mutation escape scores. Escape scores were averaged across replicates that passed quality
724 control.

725 Site-level escape scores were computed as the sum of mutation escape scores per Gn-head residue.
726 These scores were used as antibody-specific features to generate a matrix $\boldsymbol{A}_{N\times M}$, where N is the
727 number of antibodies and M is the number of valid positions. Non-surface residues on Gn-head
728 were removed from the analysis. We calculated the pairwise similarities, defined as the square root
729 of the Jensen-Shannon divergence (scipy, v1.11.2) between the feature vectors of two antibodies.
730 The dissimilarity (1.0 - similarity) matrix were used to build a k-nearest neighbor graph (k = 6) and
731 clustered into epitope groups using Leiden algorithm (leidenalg, v0.10.2) with resolution=2.5. These
732 clusters are then refined by integrating structural mapping, V(D)J germline usage, and neutralization
733 data to define biologically meaningful epitope groups.

734 **Authentic virus neutralization assay**

735 Neutralizing activity of mAbs against authentic SFTSV was measured using a FRNT. The four
736 representative SFTSV strains used for testing include HBMC16, WCH, HNXY2017-50, and
737 HNXY2017-66.[18] Briefly, serially diluted mAbs were incubated with SFTSV virions for 1 hour at
738 37°C. The mixture was added to Vero cells and incubated for 1.5 hours at 37°C. Cells were then
739 cultured for 3.5 days in DMEM containing 1.25% methylcellulose. After fixation with 3.7%
740 paraformaldehyde for 30 minutes, cells were stained with an anti-SFTSV NP primary antibody,
741 followed by an HRP-conjugated anti-mouse secondary antibody (Applygen, C1308). Staining was
742 developed using a DAB substrate (TIANGEN, PA110). Plaque numbers were recorded, and $FRNT_{50}$
743 values were calculated.

744 ***In vivo* SFTSV Challenge Experiment**

745 Mouse studies were conducted as previously described.[18] To assess the prophylactic efficacy,
746 *IFNAR1*$^{-/-}$ mice received a single intraperitoneal (IP) injection of 5 mg/kg of each mAb or a human
747 IgG1 isotype control antibody one day before IP inoculation with 20 FFUs of SFTSV HBMC16.
748 Mice were monitored daily for clinical signs, body weight, and mortality for over 12 days. Weight
749 data are expressed as percentages of initial weight. Serum samples were collected at 3 days post-

750 infection (dpi) for viral load analysis. The therapeutic assessment was largely identical to the
751 prophylactic experiment described above, except that administration occurred one day post-
752 infection. Serum was collected at 3 and 5 dpi for viral load quantification. At 5 dpi, four mice per
753 group were euthanized, and spleen, lung, and liver samples were harvested for viral load
754 determination.

755 **RT-qPCR assay**

756 Total RNA from tissues was extracted using the RNAprep Pure Cell Kit (TIANGEN, DP430).
757 Intracellular viral RNA was quantified by RT-qPCR targeting the SFTSV L segment with primes:
758 SFTSV-L-F: 5′-CTCACTCATGCCCTCAACGA-3′ and SFTSV-L-R: 5′-
759 GATGAACTCACCAGCCCTGC-3′. For serum samples, RNA was extracted with the TIANamp
760 Virus RNA Kit (TIANGEN, DP315-R), and viral load was quantified using primers targeting the
761 SFTSV S segment: SFTSV-S-F: 5′-AGCCTAATTGGATATGTCAAATTGC-3′ and SFTSV-S-R: 5′-
762 CGGGTGAAGTGGCTGAAGG-3′.

763 **Protein expression and purification for structural analysis**

764 Expression constructs encoding the ectodomains of SFTSV Gn or Gc were transiently transfected
765 into HEK293F cells using polyethylenimine (Polysciences). Culture supernatants were harvested 7
766 days post-transfection, concentrated, and exchanged into binding buffer (25 mM Tris-HCl, pH 8.0,
767 200 mM NaCl). Proteins were first purified by Ni-NTA affinity chromatography, followed by size-
768 exclusion chromatography on a Superose 6 Increase column in final buffer (20 mM HEPES, pH 7.2,
769 150 mM NaCl). The Gn-head domain was expressed and purified similarly. Antibody Fabs were
770 expressed and purified as previously described.[52]

771 **Cryo-EM sample preparation, data collection and model building**

772 For the preparation of the complexes, the purified HB29-Gn-head was mixed with a 1.5-fold molar
773 excess of fab BD70-4003 and BD70-4017, BD70-4008-fab and BD70-4017, BD70-4003, BD70-
774 4008-fab separately, incubated on ice for 40 min and injected onto a Superdex 200 Increase 5/150
775 column (Cytiva) equilibrated with buffer 1× PBS. SDS-PAGE analysis confirmed the formation of
776 the HB29-Gn-head-3-17, HB29-Gn-head-8-17, HB29-Gn-head-3, HB29-Gn-head-8 complexes in
777 a stoichiometric ratio respectively.

778 An aliquot of 4 µL protein sample of complex at a protein concentration of 0.5 mg/mL was loaded
779 onto a glow-discharged 300 mesh grid (Quantifoil Au R1.2/1.3). The grids were blotted with a filter
780 paper at 4 °C and 100% humidity,[53] and flash-cooled in liquid ethane using a Thermo Fisher Vitrobot
781 Mark IV and screened using a 200 KV Talos Aectica.

782 Cryo-EM datasets were collected on a 300kV Thermo Fisher Titan Krios G4 electron microscope
783 equipped with a Falcon 4 camera and a selectris X energy filter (GIF: a slit width of 10eV). The
784 micrographs were collected at a calibrated magnification of x130,000 using the EPU software
785 (Thermo Fisher Scientific), yielding a pixel size of 0.95 Å at object scale. Movies were recorded at
786 an accumulated electron dose of $60e^{-}Å^{-2}\ s^{-1}$ on each micrograph that was fractionated into a stack of
787 40 frames with a defocus range of -1.0 µm to -2.0 µm.

788 Data processing was performed using cryoSPARC (v4.7.1).[54] The data underwent several steps
789 including Motion Correction, CTF Estimation, Create Templates, Template Picker, Extract from
790 Micrographs, 2D classification, 2D selection for Ab-initio Reconstruction, and subsequent
791 Homogeneous Refinement. To enhance the density around the HB29-Gn-head-Fab region, local
792 refinement was conducted using UCSF ChimeraX (v1.7)[55] and cryoSPARC. Structural modeling
793 and refinement were performed using WinCoot (v0.9.4.1)[56] and Phenix (v1.21.2).[57] Figures were
794 generated using UCSF ChimeraX (v1.7).[58]

795 **QUANTIFICATION AND STATISTICAL ANALYSIS**

796 SPR assays were performed in two biological replicates. Binding data were analysed with the
797 Biacore Insight Evaluation Software using a 1:1 binding model. Neutralization assays were
798 performed in at least two biological replicates. The half-maximal inhibitory/neutralization
799 concentrations (IC_{50}/$FRNT_{50}$) were derived from curve fitting based on a four-parameter logistic
800 regression model.

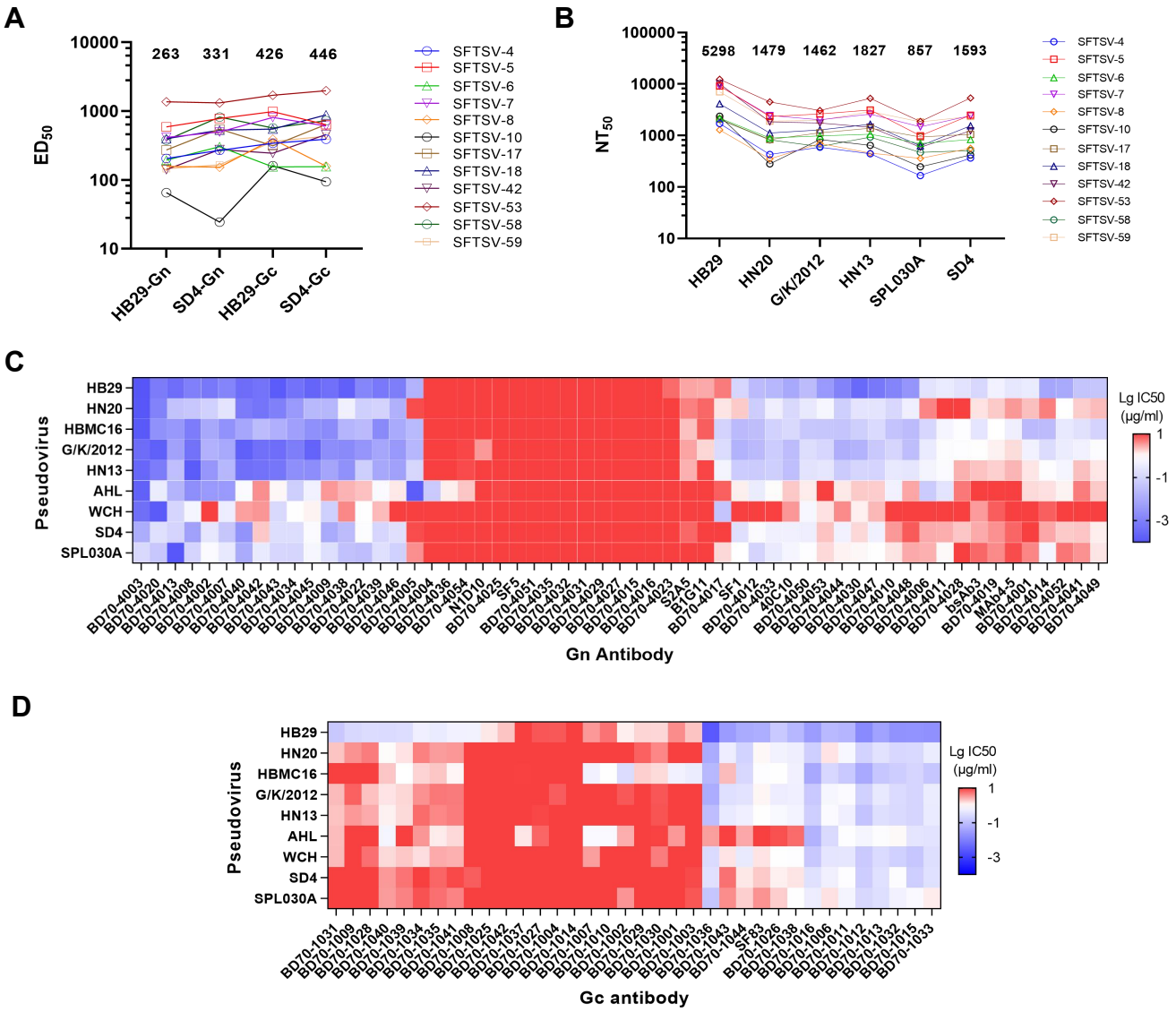

Figure 1. Identification of broad neutralizing antibodies from SFTSV-infected convalescents

(A) The median effective dose (ED_{50}) of plasma from SFTSV-infected convalescents was determined by ELISA. The average value of each group was marked.

(B) The half maximal neutralization titre (NT_{50}) of plasma against VSV-based SFTSV pseudoviruses.

(C-D) Neutralizing median inhibition concentration (IC_{50}, μg/ml) of SFTSV Gn (C) or Gc (D) antibodies using VSV-based pseudoviruses. Neutralization assays were conducted in at least two biological replicates.

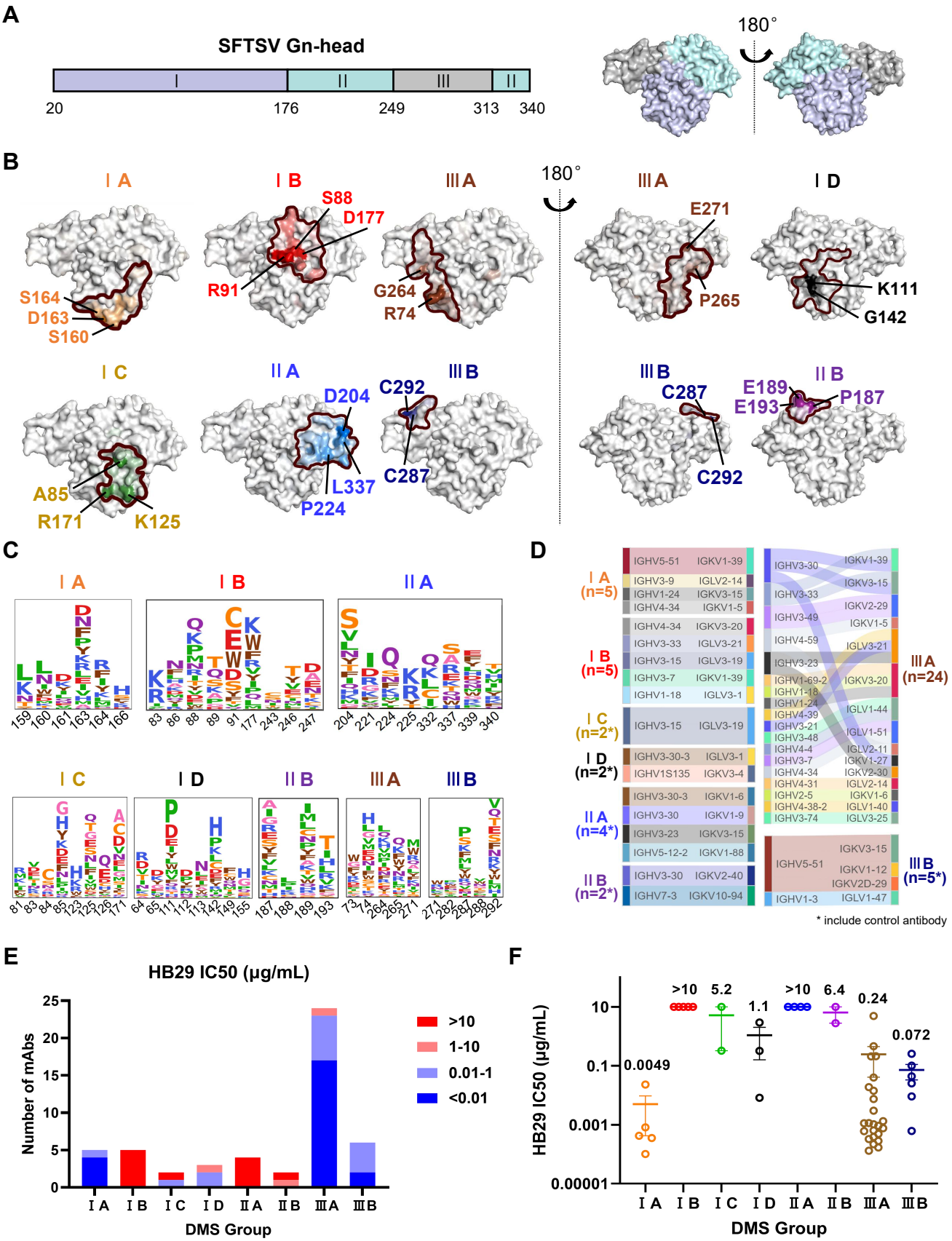

Figure 2. Epitope analysis of all Gn antibodies by yeast DMS

(A) Structural schematic of SFTSV Gn-head. The left panel illustrates the delineation of the three domains, colored in blue-white (I), pale cyan (II), and gray (III), respectively; the corresponding structural schematic is shown in the right panel (PDB: 5Y10).

(B) Structural projections and key epitope annotations of the eight DMS groups with different colors.

The region outlined by the curved line corresponds to the epitope of each respective group. In the structural projection, amino acid residues with higher DMS scores are displayed in darker colors.
(C) Average escape scores of antibodies in eight groups. Colors are assigned according to the type of amino acids, and the heights of the letters in the logo plot indicate escape scores. Residues are numbered based on Gn-head numbering.
(D) The gene analysis of the antibodies in eight groups. Sankey diagram was generated to visualize the correspondence between heavy and light chains for the antibody genes in each group, with asterisks indicating the inclusion of control antibodies.
(E-F) Statistical analysis of the number (E) and IC_{50} values (mean SEM) (F) for neutralization against the HB29 strain across DMS-classified antibody groups was performed.

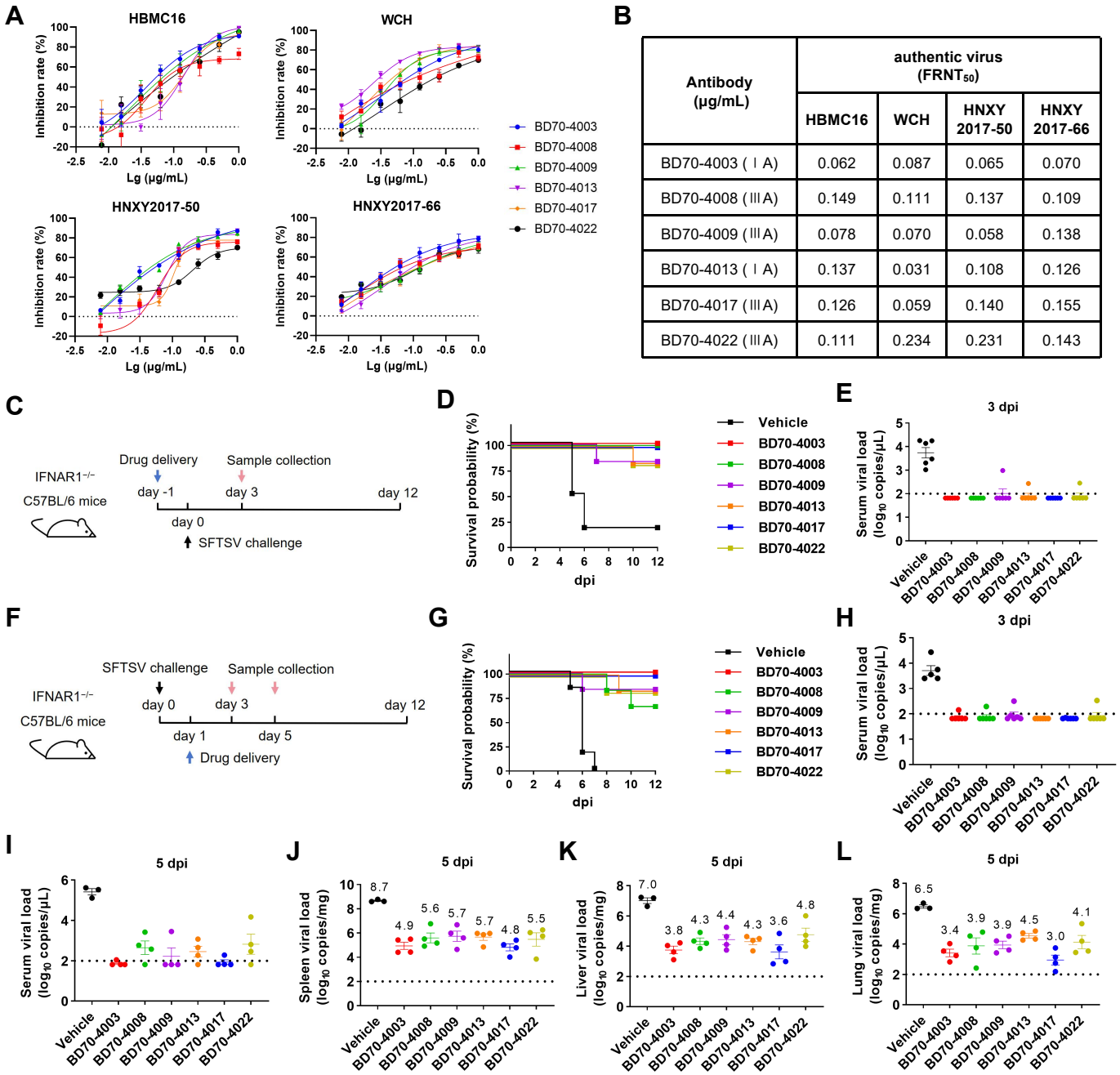

Antibody (μg/mL)	authentic virus ($FRNT_{50}$)			
	HBMC16	WCH	HNXY 2017-50	HNXY 2017-66
BD70-4003 (ⅠA)	0.062	0.087	0.065	0.070
BD70-4008 (ⅢA)	0.149	0.111	0.137	0.109
BD70-4009 (ⅢA)	0.078	0.070	0.058	0.138
BD70-4013 (ⅠA)	0.137	0.031	0.108	0.126
BD70-4017 (ⅢA)	0.126	0.059	0.140	0.155
BD70-4022 (ⅢA)	0.111	0.234	0.231	0.143

Figure 3. MAb-mediated protection of authentic virus challenge *in vitro* and *in vivo*

(A-B) The neutralization activity of six selected mAbs against four SFTSV authentic virus. The $FRNT_{50}$ was calculated using the equation of log [inhibitor] versus response-variable slope (four parameters) method. Data were shown as mean SD values from three biologically independent replicates.

(C and F) Schematic of the design for the HBMC16 challenge experiment in mice. In prophylactic groups (C), 5 mg/kg mAb was administered intraperitoneally and challenged by HBMC16 intraperitoneally 1 day later (C). In therapeutic groups (F), antibodies were given intraperitoneally 1 day after virus challenge. Each group consists of 6 mice.

(D and G) Survival curves of mice in each group.

(E, H and I) Viral load in the serum of mice in each group.

(J-L) Viral load (mean SD) of mice challenged by HBMC16 in spleen (J), liver (K), or lung (L). Each point corresponds to samples from a mouse. The limit of detection is about 1.81×10^2 copies/g and is shown as the dashed line.

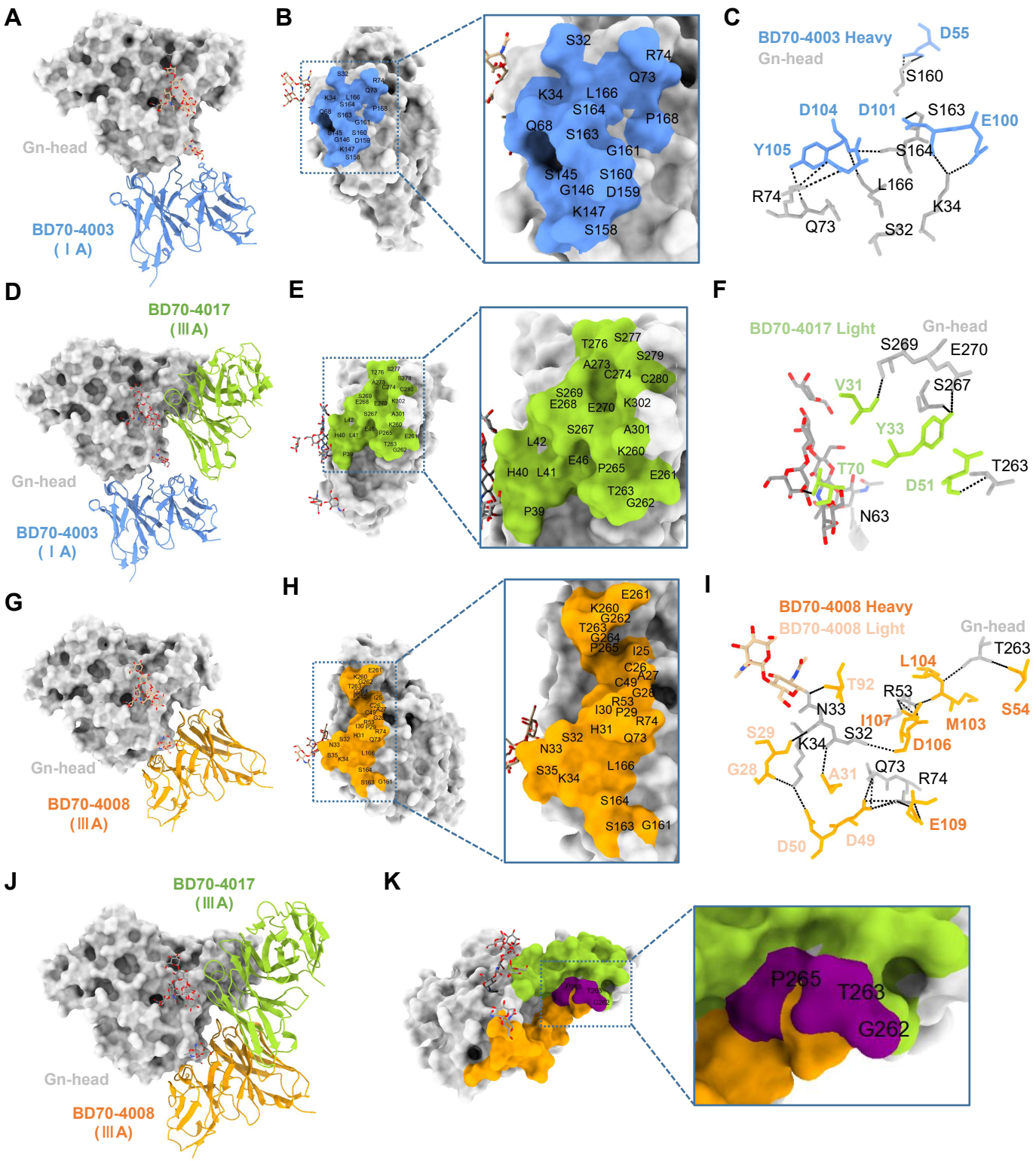

Figure 4. Cryo-EM structure of Gn antibodies bound to HB29-Gn-head

(A, D, G and J) Aligned structures of BD70-4003 (A), BD70-4003/BD70-4017 (D), BD70-4008 (G) and BD70-4008/BD70-4017 (J) on SFTSV Gn-head. BD70-4003, BD70-4008 and BD70-4017 are colored in blue, orange, and green, respectively. Gn-head is colored in gray.

(B, E and H) Surface representation of the contact residues on Gn-head interacting with BD70-4003 (B), BD70-4017 (E) and BD70-4008 (H).

(C, F and I) Interactions between the heavy-chain and light-chain BD70-4003 (C), BD70-4017 (F) and BD70-4008 (I) and Gn-head. Residues of Gn-head, BD70-4003, BD70-4008 or BD70-4017 are gray, blue, orange, and green, respectively.

(K) The overlapping epitopes of BD70-4008 and BD70-4017 are labeled in purple.

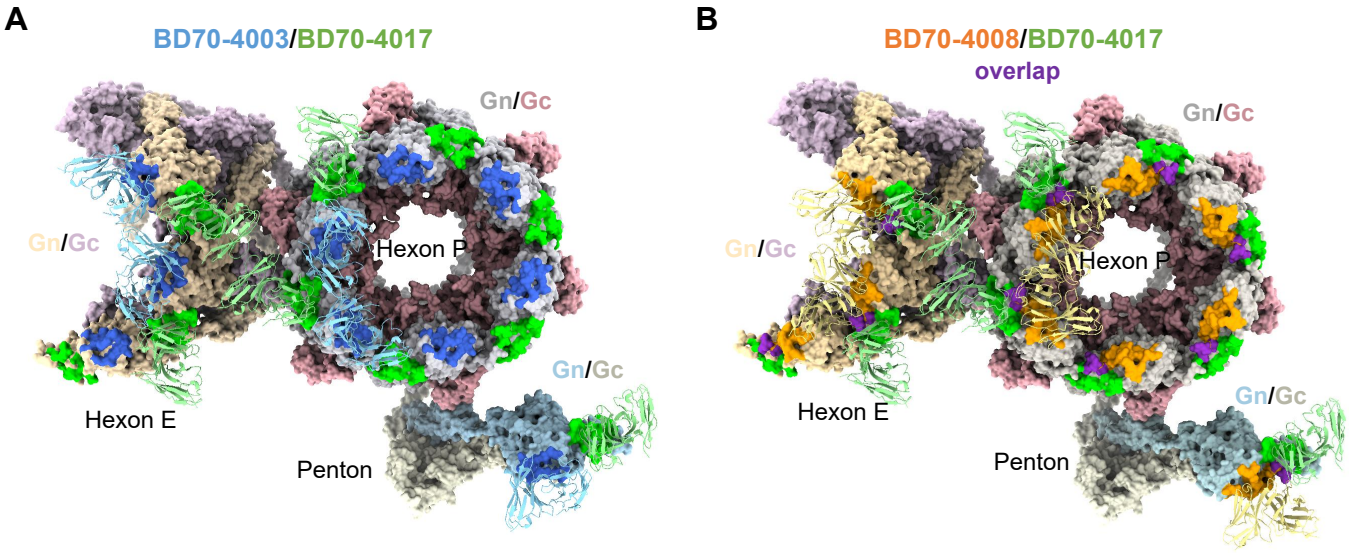

Figure 5. Docking of three antibodies onto the surface of the SFTSV virion

Docking of BD70-4003/BD70-4017 (A) and BD70-4008/BD70-4017 (B) onto the surface of SFTSV virion (PDB: 8I4T). BD70-4003, BD70-4008 and BD70-4017 are colored in blue, orange, and green, respectively. The binding sites of mAbs on SFTSV virion are labeled with colors within the same palette.